Thermal Unfolding of a Llama Antibody Fragment: A Two-State Reversible Process †

ARTICLE *in* BIOCHEMISTRY · FEBRUARY 2001

Impact Factor: 3.02 · DOI: 10.1021/bi0009082 · Source: PubMed

Thermal Unfolding of a Llama Antibody Fragment: A Two-State Reversible Process[†]

Janice M. J. Pérez,[‡] Jean G. Renisio,[§] Jeanine J. Prompers,[‡,||] Chris J. van Platerink,[‡] Christian Cambillau,[§] Hervé Darbon,*[,§] and Leon G. J. Frenken*[,‡]

Unilever Research, Olivier van Noortlaan 120, 3133 AT Vlaardingen, The Netherlands, and Architecture et Fonction des Macromolécules Biologiques, CNRS, 31 Chemin Joseph Aiguier, 13402 Marseille Cedex 20, France

Received April 20, 2000

ABSTRACT: Camelids produce functional "heavy chain" antibodies which are devoid of light chains and CH1 domains [Hamers-Casterman, C., et al. (1993) *Nature 363,* 446−448]. It has been shown that the variable domains of these heavy chain antibodies (the V_{HH} fragments) are functional at or after exposure to high temperatures, in contrast to conventional antibodies [Linden van der, R. H. J., et al. (1999) *Biochim. Biophys. Acta 1431,* 37−44]. For a detailed understanding of the higher thermostability of these V_{HH} fragments, knowledge of their structure and conformational dynamics is required. As a first step toward this goal, we report here the essentially complete ^{1}H and ^{15}N NMR backbone resonance assignments of a llama V_{HH} antibody fragment, and an extensive analysis of the structure at higher temperatures. The H−D exchange NMR data at 300 K indicate that the framework of the llama V_{HH} fragment is highly protected with a ΔG_{ex} of >5.4 kcal/mol, while more flexibility is observed for surface residues, particularly in the loops and the two outer strands (residues 4−7, 10−13, and 58−60) of the β-sheet. The CD data indicate a reversible, two-state unfolding mechanism with a melting transition at 333 K and a ΔH_m of 56 kcal/mol. H−D exchange studies using NMR and ESI-MS show that below 313 K exchange occurs through local unfolding events whereas above 333 K exchange mainly occurs through global unfolding. The lack of a stable core at high temperatures, observed for V_{HH} fragments, has also been observed for conventional antibody fragments. The main distinction between the llama V_{HH} fragment and conventional antibody fragments is the reversibility of the thermal unfolding process, explaining its retained functionality after exposure to high temperatures.

One of the primary goals of antibody engineering for biotechnological and medical applications is to minimize the size of the antigen-binding protein (*1*, *2*), in order to improve its production, stability, and in vivo properties, e.g., tissue penetration and blood clearance. These factors are important in particular for applications in bulk products, e.g., large-scale bioaffinity chromatography, consumer products (*3*), and therapeutics. The smallest antigen-binding fragments are the (single-chain) Fv[1] domains, consisting of the variable domains of the heavy (V_H) and light (V_L) chains. These recombinant fragments are stable at physiological temperatures and are expressed in *Escherichia coli* at much higher levels than the recombinant Fab fragments (*4*). It has been shown that the scFv fragments can be further stabilized by engineering of disulfide bonds between the V_H and V_L domains (*5*). However, the production level of functional (sc)Fv fragments is not yet in the range to allow a large variety of biotechnological applications, e.g., in consumer products and industrial processes (*3*).

Several years ago, a new class of antibodies, lacking the light chains and CH1 domains, was discovered in camelids (*6*, *7*). These "heavy chain" antibodies provided a natural solution for size reduction of an antibody fragment, while keeping the level of its affinity for the antigen as high as possible. In contrast to V_H fragments of "conventional" antibodies, the V_{HH} fragments from camelid heavy chain antibodies are highly water-soluble. Hydrophobic to hydrophilic amino acid substitutions [residues 37 and 44−47, Kabat numbering (*8*)] at the surface normally facing the V_L domain are most likely important for this change in solubility (*8*). This assumption has been corroborated by the "camelization" of a human V_H domain (*10*−*12*). Interestingly, we

[†] This work was supported by European Community BIOTECH Grant BIO4-CT98-048.

* To whom correspondence should be addressed. L.G.J.F.: phone, +31-10-4606569; fax, +31-10-4605383; e-mail, Leon.Frenken@unilever.com. H.D.: phone, +33-491-16-45-35; fax, +33-491-16-45-36; e-mail, herve@afmb.cnrs-mrs.fr.

[‡] Unilever Research.

[§] Architecture et Fonction des Macromolécules Biologiques, CNRS.

[||] Current address: Carlson School of Chemistry, Clark University, 950 Main St., Worcester, MA 01610-1477.

[1] Abbreviations: V_H, variable fragment from the heavy chain of a conventional antibody; V_L, variable fragment from the light chain of a conventional antibody; V_{HH}, variable fragment from a camelid heavy chain antibody; Fv, heterodimer consisting of a V_H fragment and a V_L fragment; Fab, heterodimer consisting of the light chain and variable and first constant domain of the heavy chain; hCG, human chorionic gonadotropin; V_{HH}-H14, llama V_{HH} fragment against hCG; CD, circular dichroism; NMR, nuclear magnetic resonance; NOESY, nuclear Overhauser enhancement spectroscopy; TOCSY, total correlation spectroscopy; HSQC, heteronuclear single-quantum coherence spectroscopy; FHSQC, fast HSQC; TPPI, time-proportional phase incrementation; NOE, nuclear Overhauser effect; ESI-MS, electrospray ionization mass spectrometry.

10.1021/bi0009082 CCC: $20.00
Published on Web 12/13/2000

found that the llama V_{HH} fragments can be produced at very high levels (>1 g/L) by the yeast *Saccharomyces cerevisiae* (*13*), allowing a wide range of biotechnological applications.

Despite a substantial amount of structural information about V_H domains as part of (sc)Fv or Fab fragments (*14*), relatively little is known about the structure and stability of isolated V_H domains. So far, only the solution structure of a "camelized" human V_H domain has been determined (*11*). This engineered fragment yielded slightly better expression levels and was more soluble than the conventional V_H fragment, allowing structure determination by NMR. In addition, X-ray structures of four camelid V_{HH} fragments have been determined: a llama V_{HH} antibody fragment against the α-chain of human chorionic gonadotropin hormone (hCG) (*15*), a llama V_{HH} fragment in complex with an azo dye [reactive red-6 (RR-6)] (*16*), a camel V_{HH} fragment in complex with lysozyme (*17*), and a camel V_{HH} fragment against RNAse A (*18*). In all cases, a typical immunoglobulin fold consisting of a β-sheet scaffold was found. However, some of the antigen-binding loops (CDR 1 and 2) deviate from the canonical structures described for the V_H domain of conventional antibodies.

Recently, a number of llama V_{HH} antibody fragments has been characterized biochemically (*19*). Remarkably, incubation of these V_{HH} fragments for 2 h at ≤353 K had no significant effect on the binding capability of most of the llama V_{HH} fragments, while mouse monoclonal antibodies were already completely inactivated. Moreover, two llama V_{HH} fragments against the azo dye RR-6 were still functional in a binding assay performed at 363 K (*19*). To obtain more insight into the structural parameters underlying the intrinsic stability of llama V_{HH} fragments, we report here the ^1H and ^{15}N NMR assignments of the llama V_{HH} fragment H14, raised against the α-subunit of hCG, for which the crystal structure has already been determined (*15*). The kinetic mechanism of thermal unfolding at higher temperatures of the anti-hCG V_{HH} fragment has been established with a diversity of biophysical techniques such as NMR spectroscopy, CD, and ESI-MS. We have shown that in contrast to the conventional antibodies V_{HH}-H14 is able to (un)fold reversibly, providing direct evidence of the retained functionality of llama V_{HH}'s after exposure to high temperatures.

MATERIALS AND METHODS

Proteins. Recombinant anti hCG V_{HH}-H14 was produced in *S. cerevisiae* and purified as described previously (*15*). Recombinant, uniformly ^{15}N-labeled V_{HH}-H14 was produced by using ^{15}N-labeled ammonium sulfate (99% ^{15}N, Cambridge Isotope Laboratories) as the sole nitrogen source.

CD Spectroscopy. Circular dichroism spectroscopy was performed on a Jobin-Yvon CD6 Dichrograph. The spectra were recorded on unlabeled V_{HH}-H14 samples in buffer containing 10 mM sodium acetate and 100 mM NaCl (pH 4.6). The near-UV data (250−350 nm) were measured at a protein concentration of 22 μM in 10 mm path length circular quartz cuvettes and the far-UV data (190−250 nm) at a concentration of 0.1 mM in 1 mm path length cuvettes. NMR relaxation experiments performed at 3 mM showed that the protein exists predominantly as a monomer at this concentration (H. Darbon, personal communication). The calibration of the instrument was performed with a standard solution of 1.25 g/L isoandrosterone in dioxane. In addition, a daily checking procedure was performed using a 1.00 g/L (+)-10-camphorsulfonic acid solution in water. Five spectra were averaged, corrected for the buffer solution, recalculated in mean residual molar ellipticity (θ) units (degrees times square centimeter per decimole) and smoothed using Jobin-Yvon CD6 Dichro software. A temperature-controlled water bath (Neslab RTE-110) kept at 293, 313, 333, 343, and 353 K was used to change the local temperature in the cuvette holder. The equilibration time at each temperature point was 5 min.

Equilibrium thermal denaturation was monitored in both the near-UV CD region at 273 nm and the far-UV CD region at 205 nm. The former monitors tertiary structure and the latter the secondary structure. The temperature was increased from 293 to 345.5 K (363 K at 273 nm) in 0.25 K steps in approximately 2 h. The reversibility of thermal denaturation was checked by stepwise cooling of the protein solution back to 293 K. Data analysis was performed assuming a two-state N ⇔ U unfolding mechanism. The data were fitted to eq 1:

$$y = (b_f + m_f T + (b_u + m_u T)\exp\{-\Delta H_m(1 - T/T_m) + \Delta C_p[T_m - T + T\ln(T/T_m)]/RT\})/(1 + \exp\{-\Delta H_m(1 - T/T_m) + \Delta C_p[T_m - T + T\ln(T/T_m)]/RT\}) \quad (1)$$

where y represents the observed CD signal, b_f and b_u are the intercepts, m_f and m_u represent the slopes of the pre- and post-transition baselines, respectively, T is the temperature (kelvin), T_m is the midpoint transition temperature, ΔH_m is the enthalpy change for unfolding at T_m, and ΔC_p is the change in heat capacity (*20*, *21*). Thermally induced denaturation data were converted to plots of f_u, the fraction of protein in the unfolded state:

$$f_u = (\exp\{-\Delta H_m(1 - T/T_m) + \Delta C_p[T_m - T + T\ln(T/T_m)]/RT\})/(1 + \exp\{-\Delta H_m(1 - T/T_m) + \Delta C_p[T_m - T + T\ln(T/T_m)]/RT\}) \quad (2)$$

MS Sample Preparation. Unlabeled V_{HH}-H14 (1 mg) was dissolved in 1 mL of 10 mM sodium phosphate, 140 mM NaCl (pH 7.4), and 6 M guanidinium chloride and the mixture incubated on ice for 1 min. To initiate refolding, the protein solution was diluted 1:100 with 10 mM sodium phosphate (pH 7.4) and 150 mM NaCl, in D_2O. The pH meter readings were corrected for the isotope effect (*22*). After incubation for 30 min on ice, the protein solution was concentrated in an Amicon cell to 3 mL. The concentrated protein solution was dialyzed overnight against 10 mM ammonium acetate (pH 4.6) in D_2O and purified by gel filtration on a PD-10 column. The sample was further concentrated with a Centricon-3 concentrator (Amicon) to 100 μL and stored at 253 K. Just before use, the deuterated solvent was removed in a Speed-Vac evaporator. To initiate D−H exchange, the dried sample was dissolved in 10 mM ammonium acetate buffer (pH 4.6) in H_2O and incubated at the respective temperatures (296, 307, 313, 318, 323, 333, 338, 343, and 348 K) in a thermostatically controlled water bath. At appropriate time intervals, samples were quenched

Table 1: Data Acquisition Parameters of the NMR Experiments Used for the Assignment

spectrometer frequency (MHz)	experiment	spin-lock or mixing time (ms)	heteronucleus			no. of complex points			spectral width (Hz)			ref
			F_1	F_2	F_3	F_1	F_2	F_3	F_1	F_2	F_3	
500	[^{15}N,1H]-HSQC		^{15}N	^{1}H		512	2048		2534	10000		*23*−*25*
						512	2048		10136	10000		*23*−*25*
						128	2048		1824	2604		*23*−*25*
	TOCSY	80	^{1}H	^{1}H		512	2048		6009	6000		*26*
	NOESY	100	^{1}H	^{1}H		512	2048		6009	6000		*27*
	[^{15}N]-HSQC-TOCSY	70	^{15}N	^{1}H		512	2048		2534	10000		*28*, *29*
	[^{15}N]-HSQC-NOESY	100	^{15}N	^{1}H		256	2048		2534	10000		*28*, *29*
	[^{15}N]-TOCSY-HSQC	100	^{1}H	^{15}N	^{1}H	256	54	1024	2604	1824	6002	*30*
	[^{15}N]-NOESY-HSQC	100	^{1}H	^{15}N	^{1}H	256	128	1024	2604	1824	6002	*30*
			^{1}H	^{15}N	^{15}N	64	64	2048	2604	1824	1824	*30*
600	TOCSY	50	^{1}H	^{1}H		512	2048		9090	9090		*26*
		80	^{1}H	^{1}H		512	2048		9090	9090		*26*
750	[^{15}N,^{1}H]-HSQC		^{15}N	^{1}H		88	2048		2801	12500		*23*−*25*
	NOESY	100	^{1}H	^{1}H		400	1536		10000	9009		*27*
	[^{15}N]-NOESY-HSQC	100	^{1}H	^{15}N	^{1}H	100	128	1024	10000	3290	9009	*30*

by a 1:50 dilution in ice-cold 2% acetic acid. Near-UV CD experiments showed that the presence of 2% acetic acid has a negligible effect on the tertiary structure of V_{HH}-H14.

Instrumental Setup of H−*D Exchange by MS.* The ESI-MS measurements were performed on a Quattro-II (Micromass, Manchester, U.K.) mass spectrometer. Deuterated V_{HH}-H14 (1 nmol) was used in every MS measurement. The quenched samples were injected at a concentration of 20 pmol/μL. The Hamilton syringe used for the injections was wrapped in two layers of plaster to prevent heat exchange with the environment and was precooled in an ice bath. The Valco injector and the injection loop were also cooled with a plastic bag filled with ice. The source temperature was set to 323 K to aid desolvation of electrospray droplets. The nebulizer gas was led through a copper spiral cooled at 273 K. The ion spray voltage was 4 kV. The protein solution was injected at a flow rate of 10 μL/min. Spectra of the multiple charged ions were recorded in the mass range of 1100−1800 at a rate of 5 s/scan. The kinetic experiments performed in the high-temperature range (T > 333 K) were scanned with a larger mass range (600−1900) to detect higher charge states. The average molecular masses for the protein sample were calculated from the 8- and 9-fold charged molecular ion peaks using Masslynx transformation software (Micromass).

NMR Sample Preparation. For the NMR assignments, an unlabeled V_{HH}-H14 sample and a uniformly ^{15}N-labeled V_{HH}-H14 sample were prepared in a buffer containing 10 mM deuterated sodium acetate (99.5% D, pH 4.6) at protein concentrations of 3.3 mM. The samples contained 90% H_2O and 10% D_2O (99.9% D). For the hydrogen−deuterium exchange experiments, lyophilized, uniformly ^{15}N-labeled V_{HH}-H14 was dissolved in D_2O buffer [10 mM deuterated sodium acetate (99.5% D), 100 mM NaCl, and 0.02% sodium azide (pH 4.6)] to a concentration of 0.5 mM. The pH meter readings were corrected for the isotope effect (*22*).

NMR Spectroscopy. All NMR data sets used for the assignments were collected at 300 K on three different spectrometers: a Bruker 500 MHz DRX spectrometer equipped with a triple-resonance probehead (^{1}H, ^{15}N, and ^{13}C) with self-shielded triple-axis gradients, a Bruker 600 MHz AMX spectrometer equipped with a 5 mm inverse triple-resonance probehead (^{1}H, ^{15}N, and ^{13}C) with a self-shielded z-gradient coil, and a Varian Unity 750 MHz spectrometer. Details of the experiments are given in Table 1. The TOCSY experiments were performed with a spin-lock field strength of 8 kHz. Water suppression was achieved using presaturation during the relaxation delay (1.5 s), and during the mixing time in the case of NOESY experiments, or using a Watergate 3-9-19 pulse train with a gradient at the magic angle obtained by applying simultaneous x-, y-, and z-gradients prior to detection. Quadrature detection in the indirectly detected dimensions was accomplished using the TPPI or States−TPPI acquisition method (*31*).

The hydrogen exchange experiments were performed on a Bruker 600 MHz AMX spectrometer equipped with a 5 mm inverse triple-resonance probehead (^{1}H, ^{15}N, and ^{13}C) with a self-shielded z-gradient coil. Hydrogen exchange data at pH 4.6 were recorded at 300, 307, 313, and 323 K. At 300 K, 35 two-dimensional [^{15}N,^{1}H] water flip-back fast HSQC (FHSQC) spectra (*32*) were measured between 1 h and ∼2 weeks after sample preparation. The same set of experiments was repeated at pH 5.6. At 307 K, 38 FHSQC spectra were measured between 1 h and ∼1 week after sample preparation. At 313 K, 18 FHSQC spectra were measured between 1 and 20 h after sample preparation. At 323 K, all signals had disappeared already in the first spectrum recorded after sample preparation. The spectral width in the ^{15}N dimension was 1627 Hz (folding in some backbone resonances), and it was 7246 Hz in the ^{1}H dimension(s). Quadrature detection in the indirectly detected dimensions was accomplished using the States−TPPI acquisition method (*31*).

NMR Data Analysis. The Bruker spectra were processed with XWINNMR (Bruker) or Triad software (Tripos Inc.) and the Varian spectra with NMRPipe (*33*), running on Silicon Graphics workstations. All dimensions were apodized using shifted sine-bell windows and zero-filled to the next power of 2 to improve the digital resolution.

For obtaining the chemical shift assignments, spectra were analyzed with XEASY graphical software (*34*). The spin systems were first identified by a combined use of [^{15}N,^{1}H]-HSQC (*23*−*25*), TOCSY (*26*), two-dimensional [^{15}N,^{1}H]-HSQC-TOCSY (*28*, *29*), and three-dimensional [^{15}N,^{1}H]-TOCSY-HSQC experiments (*30*). Then, the sequential assignment was obtained by analyzing NOESY (*27*), two-dimensional [^{15}N,^{1}H]-HSQC-NOESY (*28*, *29*), and three-dimensional [^{15}N,^{1}H]-NOESY-HSQC spectra (*30*).

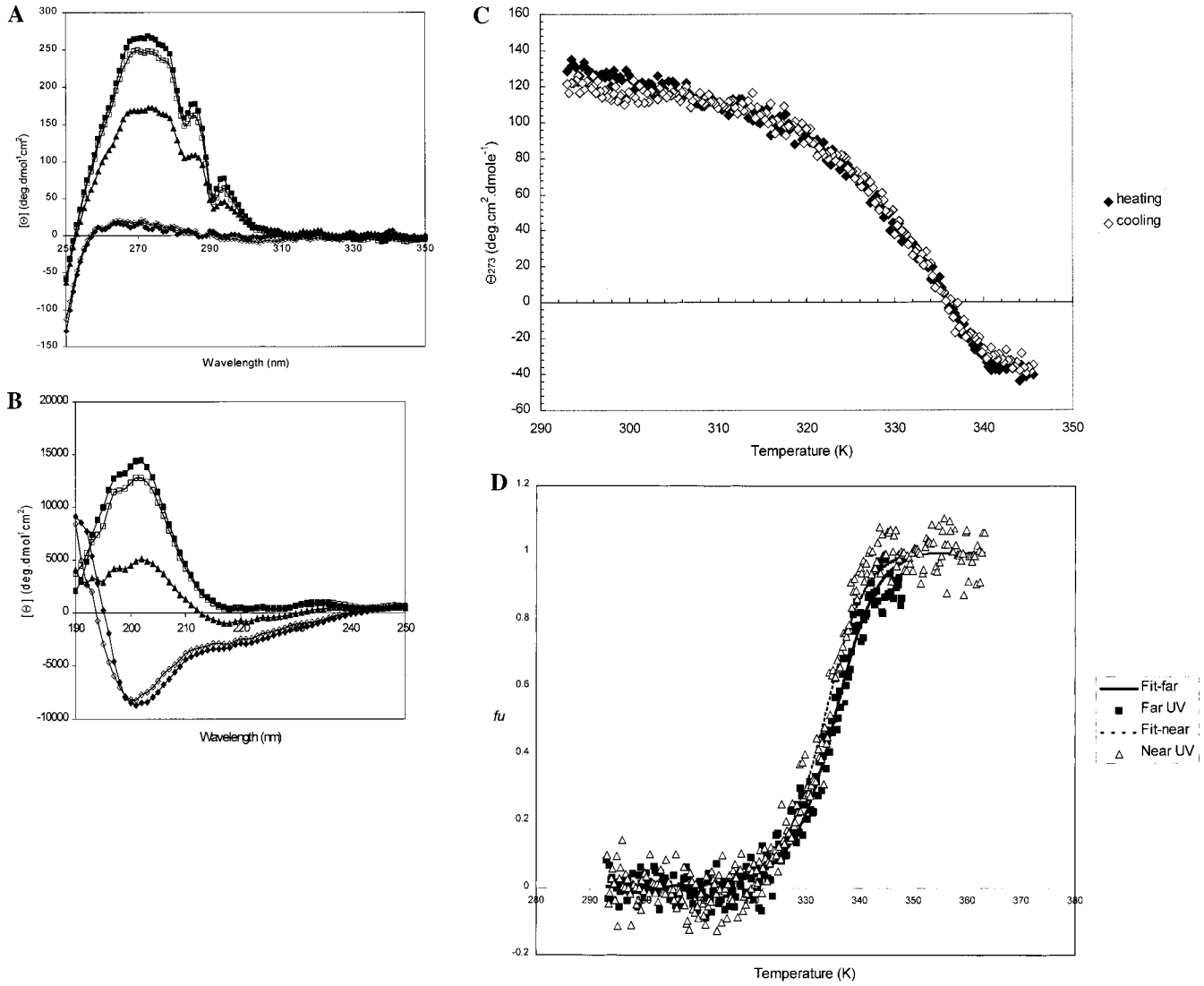

FIGURE 1: CD spectra of V_{HH}-H14 recorded in the (A) near-UV and (B) far-UV regions at increasing temperatures: (■) 293, (□) 313, (▲) 333, (◇) 343, and (◆) 353 K. (C) Thermally induced denaturation curves of V_{HH}-H14 monitored at 273 nm: mean molar residual ellipticity upon heating (◆) and upon cooling (◇). (D) Comparison of the denaturation curves monitored at 273 nm in the near-UV CD region (△) and at 205 nm in the far-UV region (■); f_u is the fraction of unfolding. The solid line represents the far-UV fit and the dotted line the near-UV fit.

Amide proton−deuterium exchange rate constants for every amide site in V_{HH}-H14 were derived from peak volumes integrated with the Triad software package (Tripos Inc.). The rate constants were calculated by fitting a single-exponential decay function to the experimental data, using a three-parameter fit to the equation

$$I(t) = I_\infty + (I_0 - I_\infty)\exp(-k_{ex}t) \quad (3)$$

where $I(t)$ is the intensity of an amide at time t after addition of D_2O to the lyophilized protein, I_0 is the intensity at time zero, I_∞ is the intensity at infinite time, and k_{ex} is the observed exchange rate constant. The parameters were fitted using the SAS package (SAS Institute Inc.), applying the Levenberg−Marquardt algorithm (*35*, *36*). For amide protons that did not exchange completely before the last experiment was finished, and for which I_∞ was not well-determined, the decay curve was fitted using a final intensity of zero. Error estimates for the rates were obtained from the standard deviations of the curve fits. The intrinsic rate constants k_{RC} were obtained using the parameters from Bai et al. (*37*). Protection factors P were then calculated according to

$$P = k_{RC}/k_{ex} \quad (4)$$

This can be related to the free energy of exchange

$$\Delta G_{ex} = -RT\ln(P) \quad (5)$$

RESULTS

Thermal Unfolding Monitored by CD Spectroscopy. To determine the stability of V_{HH}-H14, thermodynamic parameters governing the heat of denaturation have been obtained. CD spectra of V_{HH}-H14 were recorded in the near- and far-UV regions at increasing temperatures (Figure 1A,B). These spectra reveal a progressive loss in tertiary as well as in secondary structure once the temperature is increased. At 343 K, the protein is completely unfolded (Figure 1A,B). After the sample had been cooled to 293 K, spectra identical to the reference spectra at 293 K were obtained (data not shown). The reversibility of the process can also be clearly observed from the thermally induced de- and renaturation

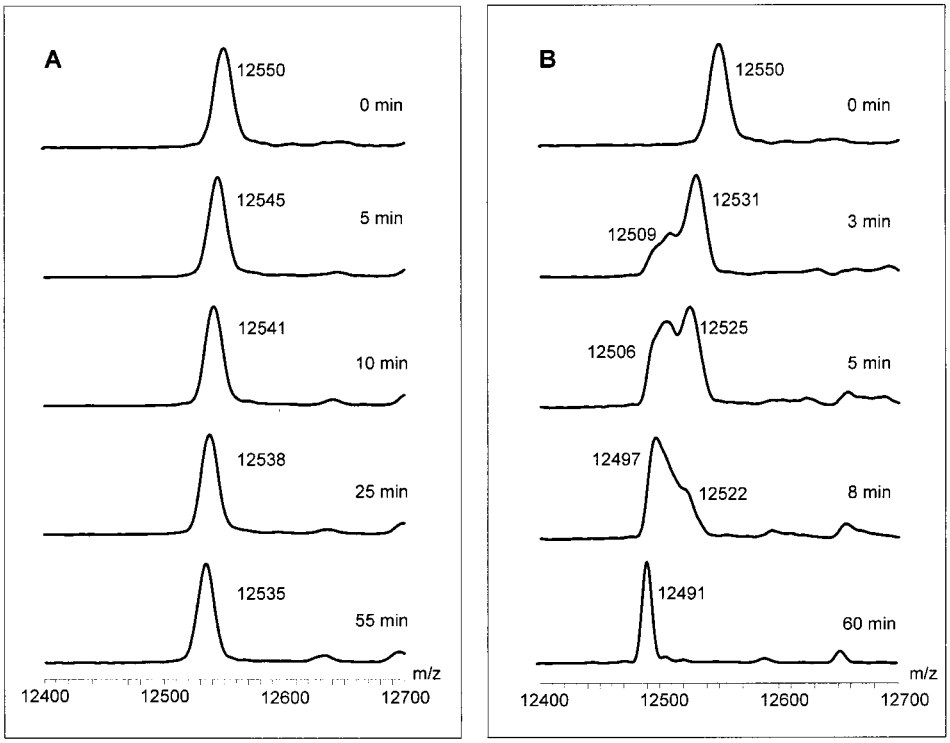

FIGURE 2: Evolution of the mass peaks as a function of the H−D exchange time period at 296 (A) and 323 K (B). In panel A, only one mass peak shifts as a function of time, and in panel B, different conformations of V_{HH}-H14 are observed. The M_w of completely deuterated V_{HH}-H14 is 12 710 Da.

curves monitored at 273 nm (Figure 1C). After cooling, the CD signal was recovered for more than 90%. The incomplete recovery of the CD signal may be due to some aggregation and/or proteolysis at elevated temperatures (C. van Vliet, personal communication). Furthermore, a single transition of denaturation was observed in the temperature range from 293 to 345.5 K monitored by the two probes: mean molar residue ellipticity at 273 nm, a probe for tertiary structure, and mean molar residue ellipticity at 205 nm, a probe for secondary structure. The denaturation profiles of the two probes coincide very well, consistent with a two-state unfolding mechanism (Figure 1D). The thermodynamic parameters were calculated by using eq 1 and assuming a ΔC_p of 0. We found a T_m of 333 ± 0.8 K and a ΔH_m of 57 ± 3 kcal/mol at 205 nm and a T_m of 333 ± 0.8 K and a ΔH_m of 55 ± 3 kcal/mol at 273 nm. Despite a lack of post-transition data at 205 nm, the thermodynamic parameters for the two probes were the same within experimental error (Figure 1D). The ΔG value could not be extracted because of the assumption that $\Delta C_p = 0$.

D−H Exchange, As Evaluated by ESI-MS. To obtain information about the population distribution of the species in solution during the thermal unfolding process of V_{HH}-H14, we performed H−D exchange experiments and subsequently analyzed the samples by ESI-MS. The experiments were performed at nine different temperatures: 296, 307, 313, 318, 323, 333, 338, 343, and 348 K. V_{HH}-H14 is composed of 117 amino acid residues with a calculated averaged molecular mass of 12 490.7 Da, assuming that the N-terminal residue is a pyroglutamine. Theoretically, 220 protons (114 backbone amide protons, 104 side chain protons, 1 proton at the N terminus, and 1 proton at the C terminus) in V_{HH}-H14 can be exchanged with deuterons. The ESI-MS experiments were all initiated with a completely deuterated protein sample. However, the molecular mass at time zero in the different experiments was approximately 130 Da lower than the theoretical molecular mass of completely deuterated V_{HH}-H14. Back exchange occurs most probably during evaporation of the solvent in the MS probe and can be attributed to the solvent-exposed/accessible residues in the protein.

The theoretical line width, including the natural isotope distribution of the molecular mass peak of V_{HH}-H14, is 8 Da. At time zero and 296 K, the line width of the molecular mass peak was approximately 16 Da, implying the coexistence of several conformers with slightly different masses. This clearly shows that the structure of V_{HH}-H14 is rather flexible under this condition, which is considered to be native.

At 296, 307, and 313 K, a unique molecular mass peak shifts to lower mass values as a function of time (Figures 2A and 3A). In sharp contrast are the observations made at higher temperatures. During the course of the experiment at ≥318 K, the molecular mass peak splits in several subpeaks (more than three). This is a clear indication that the transition temperature of V_{HH}-H14 is approached, which will lead to the appearance of different conformers (Figure 2B). The conformer with the lowest molecular mass is the completely exchanged state of V_{HH}-H14, i.e., the unfolded state. The different peaks are not completely resolved in the ESI-MS spectrum because the mass difference is only 7 Da, which is in the same range as the theoretical line width for V_{HH}-H14.

The D−H exchange rates from the ESI-MS data are ensemble averages of the exchange rates at all labile sites (side chain and backbone) in the protein. Because of the small amount of data points and the fact that the observed k_{ex} is a composite value, we limited ourselves to a qualitative

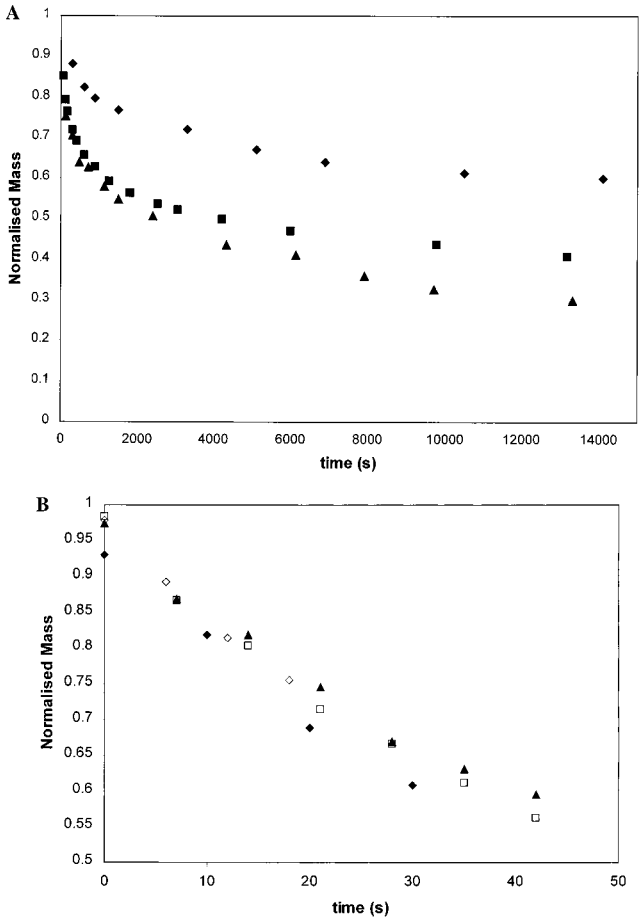

FIGURE 3: (A) D−H exchange kinetic profiles at 296 (◆), 307 (■), and 313 K (▲) measured by ESI-MS. (B) Kinetic profiles at 333 (◆), 338 (□), 338 (duplicate) (▲), and 343 K (◇).

interpretation of the ESI-MS data. The D/H exchange rates increased substantially at higher temperatures and became more uniform at >333 K (Figure 3A,B). In Figure 3B, only the initial shift of the molecular mass peak is shown. The exchange rates at >333 K is believed to be the global unfolding rate of the protein. No change in charge state distribution was observed during the thermal unfolding studies of V_{HH}-H14.

Sequential Assignment. To obtain site-specific structural information about the llama V_{HH} fragment at higher temperatures, the assignments of the ^1H and ^{15}N NMR resonances of V_{HH}-H14 are required. The spin systems identified from the TOCSY spectra were sequentially connected through either α_i-N_{i+1} or N_i-N_{i+1} correlations in the NOESY spectra and in most of the cases confirmed by β_i-N_{i+1} correlations. The sequential assignment started in the extended regions of the protein. Residues W36, F37, and R38 were easily assigned due to their downfield-shifted H^N resonance frequencies. When we started from this amino acid sequence, it was possible to assign the whole framework except for C96. In the crystal structure, C96 forms a disulfide bridge with C22, which can adopt two alternative conformations (*15*). Transitions between these conformations could take place in the slow/intermediate exchange regime, which might explain the missing assignments for C96.

Assigning the CDR regions was less trivial, most likely because of the higher flexibility of these loops. Spin systems

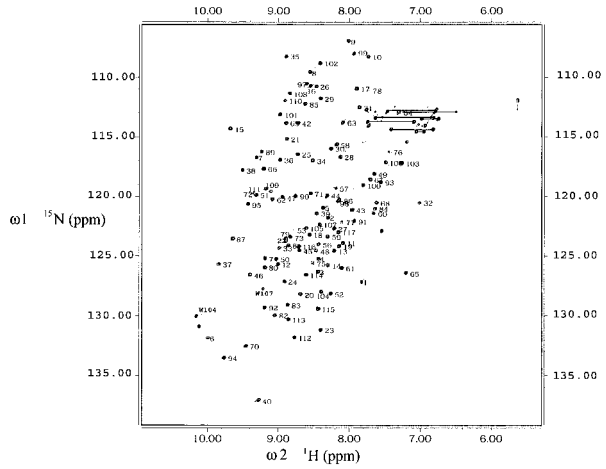

FIGURE 4: Two-dimensional [^{15}N,^{1}H]-HSQC spectrum of V_{HH}-H14. The assignments of the backbone amide $^{15}N-^1H$ correlations are indicated. Unlabeled peaks belong to side chain amide or amino groups.

were often incomplete, or only detectable in the TOCSY spectra, e.g., for Y32, or in the NOESY spectra, e.g., for W53. D54 and S55 belonging to CDR2 were not observed at all in the NMR spectra. At the end of the sequential assignment procedure, 114 of 117 amino acids were unambiguously assigned. All assignments are listed in the Supporting Information. The assigned [^{15}N,^{1}H]-HSQC spectrum is shown in Figure 4.

Amide Hydrogen Exchange, As Evaluated by NMR. Panels A and B of Figure 5 show the amide hydrogen protection factors (P) of V_{HH}-H14 obtained from the exchange data recorded at 300 K. The H−D exchange data show clearly that the amino acids in the framework of llama V_{HH}, which consists of two β-sheets in a β-sandwich type structure, have very high protection factors (>1000) with a ΔG_{ex} well over 5.4 kcal/mol, indicative of a stable structure (Figure 5). However, the residues located in the CDRs, the other loops, at the β-strand extremities and in the two outer strands of the sheets (residues 4−7 and 10−13 and residues 58−60) exchange faster (Figure 5B). The lower level of protection at the strand extremities is probably due to the weaker interaction between the strands making the residues in these regions more solvent accessible (fraying). The N-terminal strand (residues 4−7 and 10−13) is less stable probably because of irregularities in the β-strand; e.g., a β-bulge was seen in the X-ray structure. Similarly, the short strand ranging from residue 58 to 60 determined in the crystal structure is less protected because of limited stabilization through hydrogen bonds. These findings are suggestive of reduced rigidity in the structure of V_{HH}-H14. The solution structure of V_{HH}-H14 together with a complete dynamic analysis by NMR relaxation will give more insight into the flexibility of the structure and will be published separately (H. Darbon, personal communication).

The amide hydrogen exchange rates for the different residues in V_{HH}-H14 were also determined at higher temperatures: 307 and 313 K (Figure 6). While the amides in the framework are highly protected from exchange at 300 K, their degree of protection drops rapidly at higher temperatures. This is observed for the whole hydrophobic core of the protein. At 323 K, the rates of H−D exchange of the amide groups were too fast to be monitored by NMR.

Exchange Mechanism. The mechanism of H−D exchange of a labile hydrogen is depicted in the scheme below (*38*).

$$N(D) \underset{k_F}{\overset{k_U}{\rightleftharpoons}} U(D) \overset{k_{RC}}{\rightleftharpoons} U(H) \underset{k_U}{\overset{k_F}{\rightleftharpoons}} N(H)$$

The exchange rate constant can be expressed as

$$k_{ex} = (k_U k_{RC})/(k_U + k_F + k_{RC}) \quad (6)$$

There are two limiting mechanisms for exchange when $k_F \gg k_U$. In the limit where $k_F \gg k_{RC}$, and thus refolding of the transient structural opening is fast compared to the intrinsic exchange rate, the equation for the exchange rate constant is reduced to

$$k_{ex} = k_U k_{RC}/k_F \quad (7)$$

In this case, the mechanism of exchange is termed EX2 (*38*−*41*).

Under denaturing conditions when $k_F \ll k_{RC}$, the following simplification applies

$$k_{ex} = k_U \quad (8)$$

and exchange is in the EX1 limit.

H−D exchange ESI-MS data at ≤313 K showed clearly only one molecular mass peak of V_{HH}-H14 shifting in the spectrum as a function of time (Figure 2A). This observation can be explained by a fast interconversion between the native and denatured state compared to the exchange rate of amides in the denatured state, i.e., an EX2 mechanism. Consequently, a uniform proton−deuterium occupancy over the whole protein population is obtained, yielding a single peak in the mass spectrum. The NMR data at 313 K show that the exchange rates for the amino acids in the core of the protein increase and become more uniform compared to those at 300 K, but are still ranging between 0.8 and 32.1 × 10^{-3} min^{-1} (Figure 6). The HSQC fingerprint of V_{HH}-H14 at ≤313 K remains roughly the same with only minor shifts due to the temperature effect (data not shown). A large shift of the amide resonances to random coil chemical shifts, or a decay in the signal intensity, is not observed, indicating that a large fraction of the V_{HH}-H14 molecules is still structured at 313 K. This finding indicates that H−D exchange at <313 K is in the EX2 limit (*38*) and that exchange occurs mainly through local fluctuations in the native structure of the protein, in full agreement with the ESI-MS data. More evidence for an EX2 mechanism has been obtained with NMR by measuring the pH dependence of the exchange rates at 300 K. In the EX2 limit, k_{ex} is dependent on the pH, as it is proportional to the concentration of H_3O^+ and OH^- in an acid- or base-catalyzed reaction. We have assesses H−D exchange at pH 5.6, keeping the rest of the experimental conditions the same as at pH 4.6. A linear dependence (slope = 1.13) is found in a plot of $\log(k_{ex}^{pH4.6})$ against $\log(k_{ex}^{pH5.6})$ for the slowly exchanging amides, consistent with an EX2 mechanism under these conditions (Figure 7) (*42*). Therefore, the NMR data are in good agreement with the ESI-MS data.

Interestingly, at >318 K different molecular mass peaks corresponding to different conformational states of V_{HH}-H14 were observed in the ESI-MS spectra (Figure 2B). Although the resolution of the measurements is low, approximately three peaks can be discerned. The lowest-molecular mass peak is assigned to the completely exchanged population of the V_{HH}-H14 molecules, indicating that the molecules have spent enough time in the unfolded state to allow the core amide deuterons to exchange for protons. In addition, two

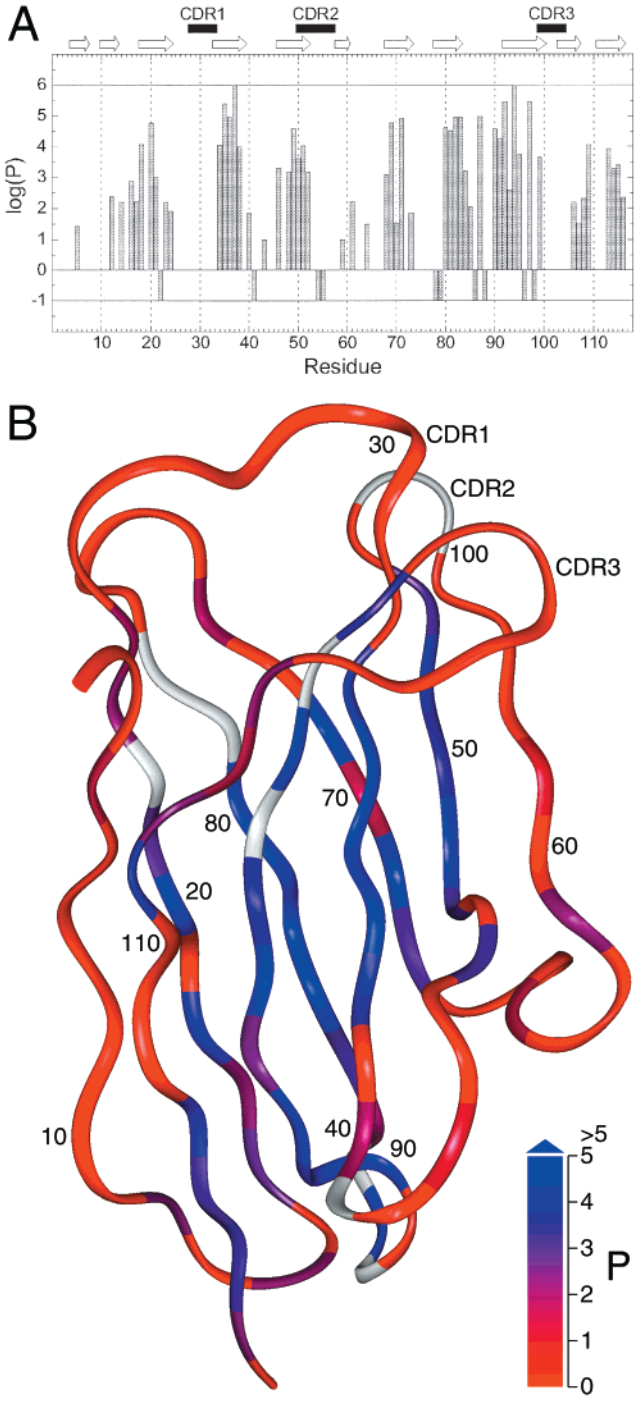

FIGURE 5: Amide hydrogen protection factors (*P*) for V_{HH}-H14 (A) plotted in a bar chart and (B) mapped on a ribbon of the crystal structure (*15*). Residue 1 is not observed in the crystal structure. A log(*P*) value of 0 was assigned to residues which exchanged too fast to be measured, and a log(*P*) value of 6 was assigned to residues which did not exchange significantly after 2 weeks. Prolines and residues with missing assignments or overlapping signals, for which the protection factor could not be determined, were given a log(*P*) value of −1 in panel A and are colored white in panel B. In panel A, residues in β-strands are indicated by arrows and residues in the CDRs are indicated by the black bars at the top of the figure. Panel B was generated with the program Insight II (MSI).

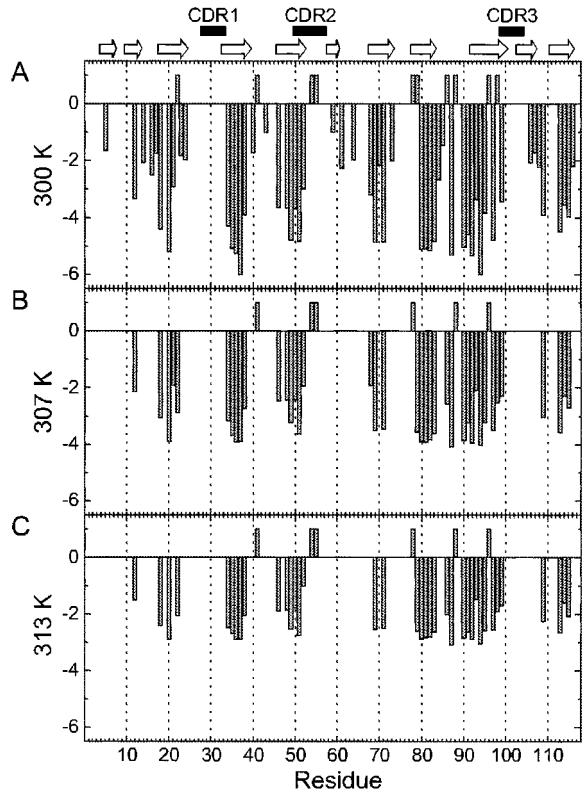

FIGURE 6: Amide hydrogen exchange rates (inverse minutes) for V_{HH}-H14 at (A) 300, (B) 307, and (C) 313 K. A log(k_{ex}) value of 0 was assigned to residues which exchanged too fast to be measured. In panel A, a log(k_{ex}) value of −6 was assigned to residues which did not exchange significantly after 2 weeks. Prolines and residues with missing assignments or overlapping signals, for which the protection factor could not be determined, were given a log(k_{ex}) value of 1. Residues in β-strands are indicated by arrows, and residues in the CDRs are indicated by black bars at the top of the figure.

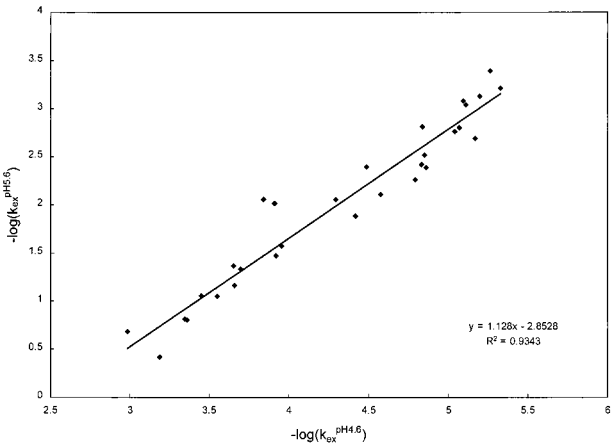

FIGURE 7: Plot of the rates of exchange of the different amide groups in V_{HH}-H14 at 300 K and at two pH values. Values of log(k_{ex}) at pH 4.6 are plotted against the values of log(k_{ex}) at pH 5.6 for the same residue. The slope is 1.13, and R^2 is 93%.

different peaks were shifting as a function of time in the ESI-MS spectra, implicating a combination of an EX1 and EX2 mechanism. In the NMR exchange experiment at 323 K, all amide protons were already completely exchanged when the first spectrum was recorded, which can be understood from the ESI-MS data. At >333 K, a sharp two-state transition between the native mass population and the unfolded mass population has been observed in the ESI-MS spectra (data not shown), consistent with the T_m value from CD (333 K). Interestingly, the exchange rates as monitored by ESI-MS at these temperatures became more uniform (Figure 3B). This clearly indicates that H−D exchange is in the EX1 limit and the measured exchange rate is equal to the rate of global unfolding. No quantitative interpretation of the ESI-MS data was attempted because of a lack of data points. On the other hand, the experiments are highly reproducible as shown in Figure 3B where the results of a duplicate experiment at 338 K are depicted.

DISCUSSION

The aim of this study was to obtain structural insight into the increased thermal stability of llama antibodies versus the conventional antibodies. For this purpose, the structure of V_{HH}-H14 has been investigated as a function of temperature by CD, NMR, and ESI-MS. We have shown by CD that llama V_{HH}-H14 displays a two-state reversible unfolding mechanism, with a melting transition at 333 K. H−D exchange by NMR at higher temperatures (≤313 K) showed increasing exchange rates, even for the residues in the hydrophobic core of the protein. This finding would imply global unfolding at these relatively low temperatures (<313 K) in contrast to the CD data. To obtain more insight into the conformational processes at ≥313 K, a D−H exchange ESI-MS study was undertaken. As ESI-MS monitors the distribution of populations during the unfolding process, NMR monitors the ensemble average. The ESI-MS data showed clearly that at <313 K D−H exchange occurs mainly through local unfolding whereas at >333 K mainly through global unfolding. This finding is consistent with the CD data and clarifies the results obtained by H−D exchange NMR.

The reversible two-state unfolding mechanism for V_{HH}-H14 is in sharp contrast with what was previously found for conventional antibodies, Mabs, Fv, and isolated V_H domains, showing irreversible denaturation at high temperatures (*43*, *44*). The ability of llama V_{HH} antibodies to refold to their native conformation explains very well the conserved functionality of llama V_{HH}'s after incubation at high temperatures (363 K). On the other hand, no significant difference between the T_m values of llama V_{HH}-H14 and two scFv fragments have been observed: the T_m value of V_{HH}-H14 = 333 K, of antilysozyme scFv = 335 K (*45*), and of the anticarbohydrate scFv = 333 K (*44*). This indicates that the thermostability of the llama V_{HH}-H14 fragment is comparable to the thermostabilities of these scFv fragments, with the only difference being its efficiency to refold upon cooling to its native conformation.

The hydrogen exchange behavior of V_{HH}-H14 is comparable to that of V_H and V_L domains in conventional antibodies (*46*−*50*). The results show that the secondary structural elements of V_{HH}-H14 are stable at 300 K (P > 1000) in the absence of quaternary interactions with the V_L domain. F37 and Y94 in V_{HH}-H14 are highly protected at 300 K with a ΔG_{ex} of >8 kcal/mol. These residues probably play an important structural role and might form the folding nucleus of single-chain V_{HH} domains. Interestingly, at higher temperatures the llama V_{HH} domain does not seem to have a stable protected nucleus but appears to be very flexible. Our results are in good agreement with the folding studies on a

single-chain Fv fragment against phosphorylcholine (*51*). In the folding intermediate of this single-chain Fv fragment, the inner β-sheet of the V_L domain is protected from exchange, while the V_H domain has no extended protected nucleus. In a more recent paper, it was shown that the V_L domain assists in folding of the V_H domain through the formation of a transient unproductive V_H-V_L domain (*52*). More details on the folding of llama V_{HH}'s are required to deepen our insight into the structural aspects of the formation of these isolated domains.

We have shown here that the structure of V_{HH}-H14 is very flexible at >300 K and that at higher temperatures (>333 K) cooperative global unfolding of the hydrophobic core of the protein takes place. A more detailed study of the dynamics of the V_{HH}-H14 solution structure will be published in a separate paper. After the denaturation of V_{HH}-H14 at 363 K, the protein is able to refold back to its biological active conformation, unlike conventional antibodies. What is still not understood is the retained functionality of some of the llama V_{HH} fragments at 363 K. Is this due to resistance to unfolding or successful refolding upon binding of the antigen? This issue is currently under investigation.

ACKNOWLEDGMENT

We thank W. Meijer and I. Schaffers for the production of V_{HH}-H14, M. ten Haaft for the purification and preparation of the H−D exchange NMR samples, A. Groenewegen and O. Bornet for assistance with the NMR measurements, E. van Velzen for assistance with the CD measurements, J. van Duynhoven, J. Haverkamp, and C. T. Verrips for stimulating discussions, and M. Egmond and G. Vuister for critical reading of the manuscript. The 750 MHz spectra were recorded at the SON NMR Large Scale Facility in Utrecht which is supported by the Large Scale Facility program of the European Union.

SUPPORTING INFORMATION AVAILABLE

A table with the resonance assignments of V_{HH}-H14. This material is available free of charge via the Internet at http://pubs.acs.org.

REFERENCES

1. Sandhu, J. S. (1992) *Crit. Rev. Biotechnol. 12*, 437−462.
2. Givol, D. (1993) *Mol. Immunol. 28*, 1379−1386.
3. Frenken, L. G. J., Hessing, J. G. M., Van den Hondel, C. A. M. J. J., and Verrips, C. T. (1998) *Res. Immunol. 149*, 589−599.
4. Plücktun, A. (1991) *Acta Biotechnol. 11*, 449−456.
5. Glockshuber, R., Malia, M., Pfitzinger, I., and Plückthun, A. (1990) *Biochemistry 29*, 1362−1367.
6. Hamers-Casterman, C., Atarhouch, T., Muyldermans, S., Robinson, G., Hamers, C., Bajyana Songa, E., Bendahman, N., and Hamers, R. (1993) *Nature 363*, 446−448.
7. Muyldermans, S., Atarhouch, T., Saldanha, J., Barbosa, J. A. R. G., and Hamers, R. (1994) *Protein Eng. 7*, 1129−1135.
8. Kabat, E., Wu, T. T., Perry, H. M., Gottesman, K. S., and Foeller, C. (1991) Sequence of Proteins of Immunological Interest, Publication 91-3242, U.S. Public Health Services, National Institutes of Health, Bethesda, MD.
9. Muyldermans, S., and Lauwereys, M. (1999) *J. Mol. Recognit. 12*, 131−140.
10. Davies, J., and Riechmann, L. (1994) *FEBS Lett. 339*, 285−290.
11. Davies, J., and Riechmann, L. (1996) *Protein Eng. 9*, 531−537.
12. Riechmann, L. (1996) *J. Mol. Biol. 259*, 957−969.
13. Frenken, L. G. J., van der Linden, R. H. J., Hermans, P. W. J. J., Bos, J. W., Ruuls, R. C., de Geus, B., and Verrips, T. (2000) *J. Biotechnol. 78*, 11−21.
14. Alzari, P. M., Lascombe, M.-B., and Poljak, R. J. (1988) *Annu. Rev. Immunol. 6*, 555−580.
15. Spinelli, S., Frenken, L., Bourgeois, D., de Ron, L., Bos, W., Verrips, T., Anguille, C., Cambillau, C., and Tegoni, M. (1996) *Nat. Struct. Biol. 3*, 752−757.
16. Spinelli, S., Frenken, L. G. J., Hermans, P., Verrips, T., Brown, K., Tegoni, M., and Cambillau, C. (2000) *Biochemistry 39*, 1217−1222.
17. Desmyter, A., Transue, T. R., Arbabi Ghahroudi, M., Dao Thi, M.-H., Poortmans, F., Hamers, R., Muyldermans, S., and Wyns, L. (1996) *Nat. Struct. Biol. 3*, 803−811.
18. Decanniere, K., Desmyter, A., Lauwereys, M., Ghahroudi, M. A., Muyldermans, S., and Wyns, L. (1999) *Structure 7*, 361−370.
19. Linden van der, R. H. J., Frenken, L. G. J., de Geus, B., Harmsen, M. M., Ruuls, R. C., Stok, W., de Ron, L., Wilson, S., Davis, P., and Verrips, C. T. (1999) *Biochim. Biophys. Acta 1431*, 37−46.
20. Agashe, V. R., and Udgaonkar, J. B. (1995) *Biochemistry 34*, 3286−3299.
21. Maier, C. S., Schimmerlik, M. I., and Deinzer, M. L. (1999) *Biochemistry 38*, 1136−1143.
22. Glasoe, P. K., and Long, F. A. (1960) *J. Phys. Chem. 64*, 188−190.
23. Bax, A., Clore, G. M., and Gronenborn, A. M. (1990) *J. Magn. Reson. 88*, 524−431.
24. Bax, A., Ikura, M., Kay, L. E., Torchia, D. A., and Tschudin, R. (1990) *J. Magn. Reson. 86*, 304−318.
25. Norwood, T. J., Boyd, J., Heritage, J., Soffe, N., and Campbell, I. (1990) *J. Magn. Reson. 87*, 488−501.
26. Bax, A., and Davis, D. G. (1985) *J. Magn. Reson. 65*, 355−360.
27. Bodenhausen, G., Kogler, H., and Ernst, R. R. (1984) *J. Magn. Reson. 58*, 370−388.
28. Susumu, M., Chitrananda, A., O'Neil Johnson, M., and van Zijl, P. C. M. (1995) *J. Magn. Reson. 108*, 94−98.
29. Talluri, S., and Wagner, G. (1996) *J. Magn. Reson. 112*, 200−205.
30. Marion, D., Driscoll, P. C., Kay, L. E., Wingfield, P. T., Bax, A., Gronenborn, A. M., and Clore, G. M. (1989) *Biochemistry 28*, 6150−6156.
31. Marion, D., Ikura, M., Tschudin, R., and Bax, A. (1989) *J. Magn. Reson. 85*, 393−399.
32. Mori, S., Abeygunawardana, C., Johnson, M. O., and van Zijl, P. C. M. (1995) *J. Magn. Reson., Ser. B 108*, 94−98.
33. Delaglio, F., Grzesiek, S., Vuister, G., Zhu, G., Pfeifer, J., and Bax, A. (1995) *J. Biomol. NMR 6*, 277−293.
34. Bartels, C., Xia, T., Billeter, M., Güntert, P., and Wüthrich, K. (1995), *J. Biomol. NMR 6*, 1−10.
35. Marquardt, D. W. (1963) *J. Soc. Ind. Appl. Math. 11*, 431−441.
36. Press, W. H., Flannery, B. P., Teukolsky, S. A., and Vetterling, W. T. (1986) *Numerical Recipes: The Art of Scientific Computing*, Cambridge University Press, Cambridge, U.K.
37. Bai, Y., Milne, J. S., Mayne, L., and Englander, S. W. (1993) *Proteins: Struct., Funct., Genet. 17*, 75−86.
38. Bai, Y., Milne, J. S., Mayne, L., and Englander, S. W. (1994) *Proteins: Struct., Funct., Genet. 20*, 4−14.
39. Chung, E. W., Nettleton, E. J., Morgan, C. J., Gross, M., Miranker, A., Radford, S. E., Dobson, C. M., and Robinson, C. V. (1997) *Protein Sci. 6*, 1316−1324.
40. Hvidt, A. A., and Nielsen, S. O. (1966) *Adv. Protein Chem. 21*, 287−386.
41. Miranker, A., Robinson, C. V., Radford, S. E., Aplin, R. T., and Dobson, C. M. (1993) *Science 262*, 896−900.
42. Skelton, N. J., Kördel, J., Akke, M., and Chazin, W. J. (1992) *J. Mol. Biol. 227*, 1100−1117.
43. Wirtz, P., and Steipe, B. (1999) *Protein Sci. 8*, 2245−2250.

44. Young, N. M., MacKenzie, R., Narang, S. A., Oomen, R. P., and Baenziger, J. E. (1995) *FEBS Lett. 377*, 135−139.
45. Yasui, H., Ito, W., and Kurosawa, Y. (1994) *FEBS Lett. 353*, 143−146.
46. Constantine, K. L., Goldfarb, V., Wittekind, M., Anthony, J., Ng, S.-C., and Mueller, L. (1992) *Biochemistry 31*, 5033−5043.
47. Constantine, K. L., Friedrichs, M. S., Goldfarb, V., Jeffrey, P. D., Sheriff, S., and Mueller, L. (1993) *Proteins: Struct., Funct., Genet. 15*, 290−311.
48. Takahashi, H., Odaka, A., Kawaminami, S., Matsunaga, C., Kato, K., Shimada, I., and Arata, Y. (1991) *Biochemistry 30*, 6611−6619.
49. Takahashi, H., Suzuki, E., Shimada, I., and Arata, Y. (1992) *Biochemistry 31*, 2464−2468.
50. Williams, D. C., Jr., Rule, G. S., Poljak, R. J., and Benjamin, D. C. (1997) *J. Mol. Biol. 270*, 751−762.
51. Freund, C., Honegger, A., Hunziker, P., Holak, T. A., and Plückthun, A. (1996) *Biochemistry 35*, 8457−8464.
52. Jäger, M., and Plückthun, A. (2000) *Protein Sci. 9*, 552−563.

BI0009082